Electrical Anisotropy and its Mitigation in Conductive Polymers Printed by Digital Light Processing

David Tilve-Martinez[a], Wilfrid Neri[a], Nicolas Vukadinovic[b], Benoit Berton[b], Alain Pénicaud[a], Jinkai Yuan[a] and Philippe Poulin*[a]*

[a] University of Bordeaux, Centre de Recherche Paul Pascal – UMR5031 CNRS, 115 Avenue Dr. Albert Schweitzer, Pessac 33600, France.

[b] Dassault Aviation, 78 quai Marcel Dassault, Saint-Cloud 98552, France.

david.tilve@crpp.cnrs.fr

philippe.poulin@crpp.cnrs.fr

Abstract:

In most 3D printing technologies, objects are realized layer by layer. This layer-by-layer construction leads to inherent anisotropic physical properties. Controlling, understanding and sometimes mitigating such anisotropy is a critical issue in the development of 3D printing. We demonstrate and quantify in this work electrical anisotropy in conductive materials processed by the so-called Digital Light Processing (DLP) method. In this method, which enjoys high resolution and high speed, layers of polymers, are successively cross-linked by UV irradiation of 2D patterns. Here, we use acrylate based resins and carbon nanotube as conductive fillers for their low percolation threshold that allows realizing conductive and still sufficiently transparent materials for UV irradiation. Conductivity parallel to the layers of 3D printed objects is found to be much greater than conductivity perpendicular to the layers. This electrical anisotropy is explained by the

high contact resistance between printed layers. High contact resistance results from the slow diffusion of carbon nanotubes from the uncured material towards the interface of the cured object. We found that implementing a delay time before curing successive layers, or decreasing the matrix viscosity with temperature, to promote diffusion of the conductive particles allow substantial reduction of the contact resistance between layers. As a result, conductivity anisotropy can be reduced by almost two orders of magnitude. This control and mitigation of conductivity anisotropy allows reconciliation of the high resolution of the DLP technology with the possibility to realize uniform 3D materials.

Keywords: Nanocomposite, Single-Walled Carbon Nanotubes, Electrical Conductivity, Anisotropy, 3D printing

Introduction

The main 3D printing technologies, including Digital Light Processing (DLP) and Fused Deposition Modelling (FDM), are based on the realization of 3D objects layer by layer[1–3]. This layer-by-layer construction generally results in anisotropic physical properties[4]. Electrical anisotropy has for instance been observed in the FDM process, and is explained by two mechanisms. One is the increase of the contact resistances between layers of polymers loaded with conductive particles[5–7] due to air gaps and lack of intimate contacts. The other one arises from filler and polymer orientation during the printing process [8–10]. Conductive composites can also be 3D printed by the DLP process if the loaded resins remain sufficiently transparent to allow photo-polymerization[11]. Such composites are particularly promising because they can enjoy better spatial resolution, complex shapes and faster printing compared to materials manufactured by FDM. Even if not yet reported, electrical conductivity anisotropy can also be expected in composites made by DLP since they are made layer by layer. Only dielectric anisotropy has been reported so far in insulating DLP printed materials. Gundrati *et al.*[12] have investigated the influence of the layer sequence on the dielectric permittivity and have observed an orientation of the polymer chains due

to compression of the uncured resin by the printing platform. Furthermore, Chakraborty *et al.*[13] have emphasized the influence of interlayer defects on the dielectric permittivity, which can arise from residual stress during the printing process.

Here, we evidence and quantitatively characterize electrical anisotropy in conductive composites made by DLP. We use acrylic resins loaded with single wall carbon nanotubes (SWCNTs). These materials are selected because they display a low percolation threshold[14–19] and a high electrical conductivity[20–24]. A low percolation threshold allows the realization of conductive resins with a small amount of carbon material[25–28] to minimize UV absorption and scattering[29]. Electrical conductivity parallel to the printed layers is shown to be much greater than the conductivity perpendicular to the layers. As demonstrated by polarized Raman spectroscopy, this electric anisotropy can not be explained here by the orientation of the fillers. Limitation of conductivity perpendicular to the layers is mainly due to the large contact resistance between printed layers. This feature is quantified by studying the influence of the thickness of the printed layers. Anisotropy of conductivity can be exceptionally high, up to two orders of magnitude. If unwanted, such high anisotropy is a serious limitation in applications, and imposes constraints on the design of conductive objects and devices. The high contact resistance between layers reflects the lack of electrical contacts established by the SWCNTs at the interface between the liquid resin and the already photo-polymerized object. Based on this understanding, we propose an approach for mitigating the anisotropy (Scheme 1). This approach consists of implementing a certain delay time before inducing photo-polymerization of a subsequent layer. This delay time allows the translational and rotational diffusion of the SWCNTs in the liquid resin at the interface of the printed object. Better electrical contacts can be established and the resistance between layers is reduced. This mitigation imposes a longer printing time. Nevertheless, the present hypothesis is also corroborated by a strong decrease in electrical anisotropy with temperature during the printing process. Increasing temperature makes the resin less viscous, allowing thereby a faster diffusion of the conductive species. Increasing printing temperature is shown to lead to less anisotropic materials while keeping fast the printing process. The present findings can therefore be particularly useful to control 3D printed materials properties that depend on a certain direction in different applications such as electromagnetic interference (EMI) shielding[30–32], structural health monitoring (SHM)[33,34] or thermoelectrics[35,36].

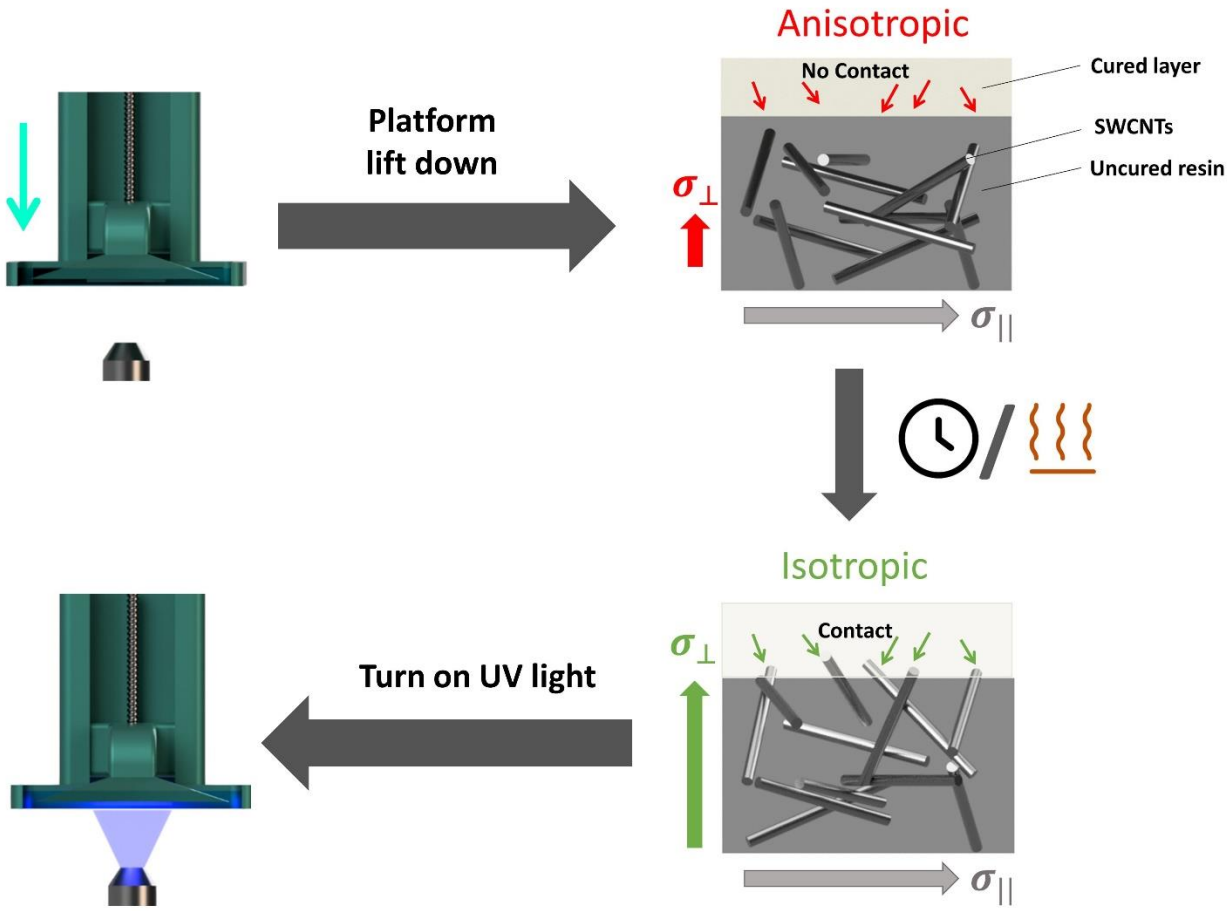

Scheme 1. Scheme of the electrical anisotropy mitigation in SWCNT composites printed by Digital Light Processing. The platform compresses the formulation avoiding the contact of the nanotubes to the cured layer. A strong anisotropy would result if the material would be cured in this state. Implementation of a delay time, or heating, allows nanotubes to migrate and rotate to the interphase, minimizing thereby the contact resistance. Last, the UV light is turned on and cross-linking of the new layer occurs.

Results and Discussion

The use of particles with a high aspect ratio enables the 3D printing of electrically conductive composites using techniques like stereolithography or DLP. Indeed, high aspect ratio particles display a low percolation threshold and allow therefore conductive networks to be realized at low concentrations. The low concentration is critical to limit UV absorption and

scattering. Homogeneous dispersion of nanoparticles is also crucial in formulating conductive resins, to limit light scattering by large aggregates. Here, we use SWCNTs because they are conductive particles with a very high aspect ratio. Their homogeneous dispersion is achieved by known methods, using surfactant and sonication. Details of their preparation and composition are given in the Experimental Section.

Furthermore, the physicochemical properties of the resulting resin were assessed, including rheology and photoreticulation (Supporting Information: S1 and S2). These analyses demonstrate that the modified resins possess favorable characteristics for printing applications.

Then, electrical properties are characterized by printing 2x2x2 mm^3 cubes with a layer thickness of 100 µm. The samples are thermally annealed at 200 ºC for 2 h after printing. Such type of annealing is known to improve electrical properties of nanocomposite fibers [37–39] and films[40,41]. The conductivity is measured with silver electrodes painted on two surfaces of the cubes, either parallel or perpendicular to the layers. Both conductivities are fitted by the scaling Equation 1:

$$\sigma = \sigma_0(\rho - \rho_c)^t \quad (1)$$

Where σ is the electrical conductivity of the composite (S m^{-1}), σ_0 is the scaling factor (S m^{-1}), ρ is the weight fraction (wt.%), ρ_c is the percolation threshold (wt.%) and t is a critical exponent that depends on the dimensionality of the system. t is expected to be about 1.8 for a 3D system, and around 1.3 in 2D[42–44].

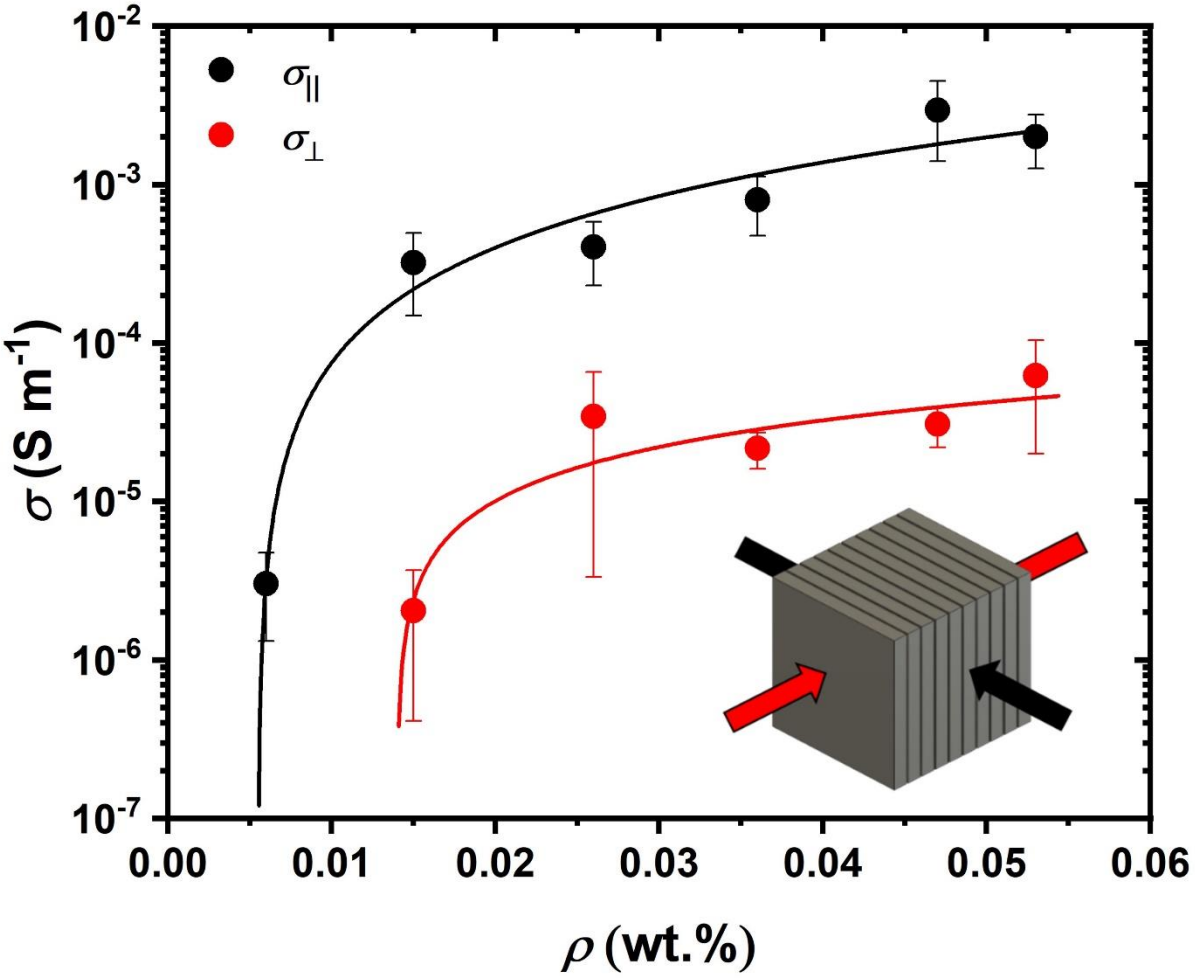

Figure 1. Electrical conductivity as a function of the weight fraction of SWCNT nanocomposites. Conductivity parallel ($\sigma_{||}$) and perpendicular ($\sigma_{\perp}$) to the layers are respectively represented by black and red curves. The data are fitted by the scaling Equation 1. Schematics of the conductivity measurements parallel (black arrows) and perpendicular (red arrows) to the 3D printing layers.

Experimental results of conductivity measurements are shown in Figure 1. The fit parameters are given in Table 1. A significant electrical anisotropy, of about two orders of magnitude, is observed. Even if observed for the first time for materials 3D printed by DLP, electrical anisotropy has been reported for materials printed by FDM or DIW. Anisotropy could be attributed in these cases to the orientation of the fillers[45,46] during the 3D printing process. The absence of extrusion in the DLP technology makes this scenario less likely, but orientation could

still result from shear during the vertical motion of the printing platform. Raman polarized scattering was performed in different composites in order to study the order parameter S[47–50] (Supporting Information: S7). The results show actually a poor degree of orientation of the fillers and confirm that the shear applied by the platform motion is not sufficient to orientate the nanotubes. Instead, the anisotropy could arise from the layer-by-layer construction of the printed objects[7,10].

Interestingly, the fitting parameters of conductivity differ for the conductivity parallel and perpendicular to the layers. Even if these parameters are deduced from fits of a limited number of points, they suggest the dominant contribution of distinct networks along different directions. t is about 1.7 for the conductivity parallel to the layers, suggesting that the network controlling the conductivity is three dimensional. By contrast, the lower value of t for the conductivity perpendicular to the layers would reflect the dominant contribution of a network of lower dimensionality such as the 2D interfacial region between printed layers. Nevertheless, this analysis has to be taken with caution considering the possible non-universality of scaling exponents due to the influence of the contact resistance between particles[51–53], and of possible aggregation mechanisms in response to attractive interactions[54].

To confirm and quantify the hypothesis that electrical anisotropy actually arises from the presence of interfacial domains between printed layers, we study the impact of the layer thickness, which is directly related to the number of interfaces per unit length.

Table 1. Parallel $\sigma_{\parallel}$ and perpendicular $\sigma_{\perp}$ conductivities of SWCNT-based composites. Fits to Equation 1.

Direction	σ_{max} (S m^{-1})	σ_0 (S m^{-1})	ρ_c (wt.%)	t
$\sigma_{\parallel}$	$2.01 \cdot 10^{-3}$	$4.60 \cdot 10^{-1}$	0.006	1.70
$\sigma_{\perp}$	$3.07 \cdot 10^{-4}$	$6.03 \cdot 10^{-4}$	0.014	0.80

We fabricated 2x2x1 mm^3 cuboid objects with different numbers of layers and similar weight fractions of nanotubes of 0.03wt%. We analyzed their electrical anisotropy (Figure 2a). The conductivity perpendicular to the layers is $\sigma_{\perp} = (15.2 \pm 9.6) \times 10^{-6}$ S m^{-1}when using 10 layers

with a thickness of 100 μm (total height 1 mm), $\sigma_{\perp}$= (3.3 ± 1.6) x 10^{-6} S m^{-1} for 50 layers of 20 μm (total height 1 mm). The ratio between the above perpendicular conductivities is 4.6, which is close to 5, the number of layers ratio. The conductivity ($\sigma_{\parallel}$) parallel to the layers is much greater than $\sigma_{\perp}$, and is weakly affected by the thickness layer. $\sigma_{\parallel}$ decreases from (4.7 ± 0.2) x 10^{-4} S m^{-1} to (2.8 ± 0.5) x 10^{-4} S m^{-1} with decreasing the layer thickness from 100 to 20 □m. Overall electrical anisotropy defined as the ratio of $\frac{\sigma_{\parallel}}{\sigma_{\perp}}$ increases from 31 to 85 for this layer thickness decrease.

The present results show that the conductivity perpendicular to the layers is limited by the contact resistance between layers. This interlayer resistance is greater than the bulk resistance of the material in between layers. The total resistance perpendicular to the layers R_{eq} can be viewed as a series of resistors with $R_{eq} = \sum R_{int}$, and where R_{int} is the net resistance of an individual layer. The values of conductivities for 10 and 50 layers respectively correspond to a net resistance R_{int} of 1.6 ± 1.0 and 1.5 ± 0.7 MΩ for each layer, almost independent of the layer thickness.

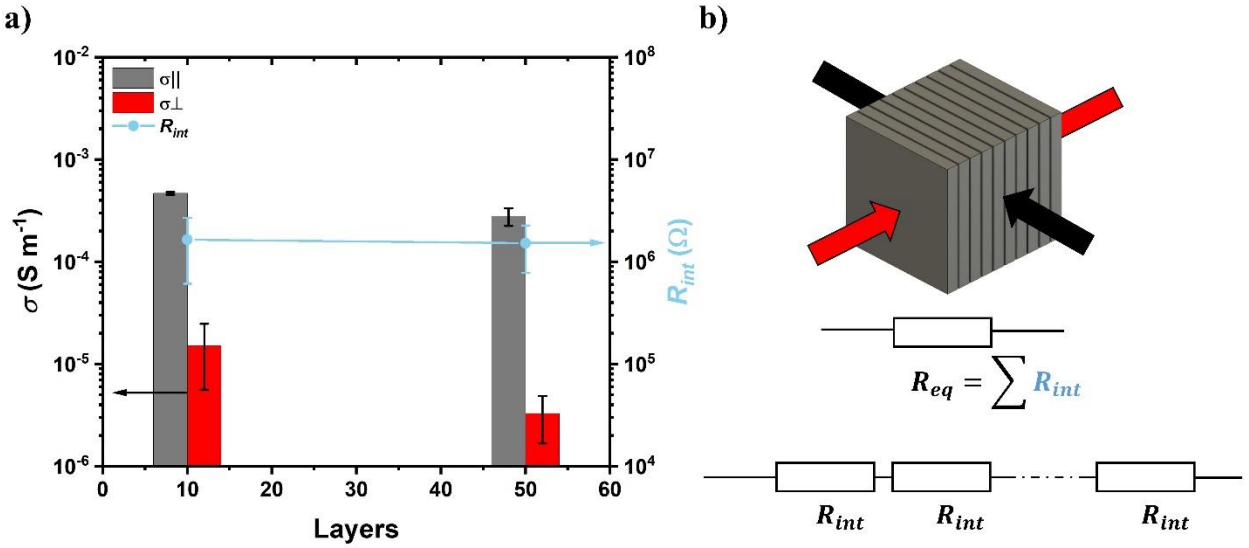

Figure 2. a) Electrical conductivity parallel (grey column) and perpendicular (red column) to the layers and the interlayer resistance (blue point) of 0.03 wt.% composite as a function of number of the layers at room temperature; b) Scheme of the layered model as a series of resistors.

The high contact resistance between layers reflects poor connectivity of nanotubes at the interface of the cured and uncured layers as printing proceeds. This poor connectivity is likely due

to the slow Brownian rotation and translation of nanotubes from the uncured resin toward the solid cured material. The Brownian rotation diffusion coefficient of a rod can be approximated to:

$$D_r = \frac{k_B T}{3\pi\eta_0 L^3} \ln(L/d) \quad (2)$$

where k_B is the Boltzmann constant, T is the temperature, η_0 is the viscosity of the fluid and L, d are the length and the diameter respectively of the nanorod[55]. The characteristic rotation time given by $1/D_r$ and using Equation 2 is 50 s for a nanotube of 1 µm in length, 1 nm in diameter, with a resin viscosity of 0.15 Pa s at room temperature.

Implementing a delay time of a few tens of seconds before curing the resin could therefore allow the establishment of better electrical contacts at the interface between layers. This expectation is experimentally confirmed by our experiments, when we imposed a delay between the time the platform reaches the printing height and the time the UV screen is activated to cross-link the next layer. As shown in Figure 3 for samples with a layer thickness of 20 µm and a fraction of nanotubes of 0.03 wt%, $\sigma_\perp$ substantially increases with the delay time. $\sigma_\perp$= (38.0 ± 18.5) x 10^{-6} S m^{-1} and (94.3 ± 14.4) x 10^{-6} S m^{-1} for respectively delay times of 30 s and 60 s, compared to (3.3 ± 1.6) x 10^{-6} S m^{-1} in absence of delay. These conductivities correspond to a decrease of R_{int} to 131.7 ± 64.2 kΩ and 53.0 ± 8.1 kΩ when delay times of 30 s and 60 s are respectively implemented, compared to 1.5 ± 0.7 MΩ for a 0 s delay. At the same time, $\sigma_\parallel$ also increases with the delay time, but this increase is much less pronounced than for $\sigma_\perp$ and the conductivity anisotropy is typically reduced by one order of magnitude.

However, printing with a long delay time increases production time and costs. For example, it can take over an hour to produce a 1 mm thick object using additive manufacturing with a delay of 45 seconds between cross-linking of each layer.

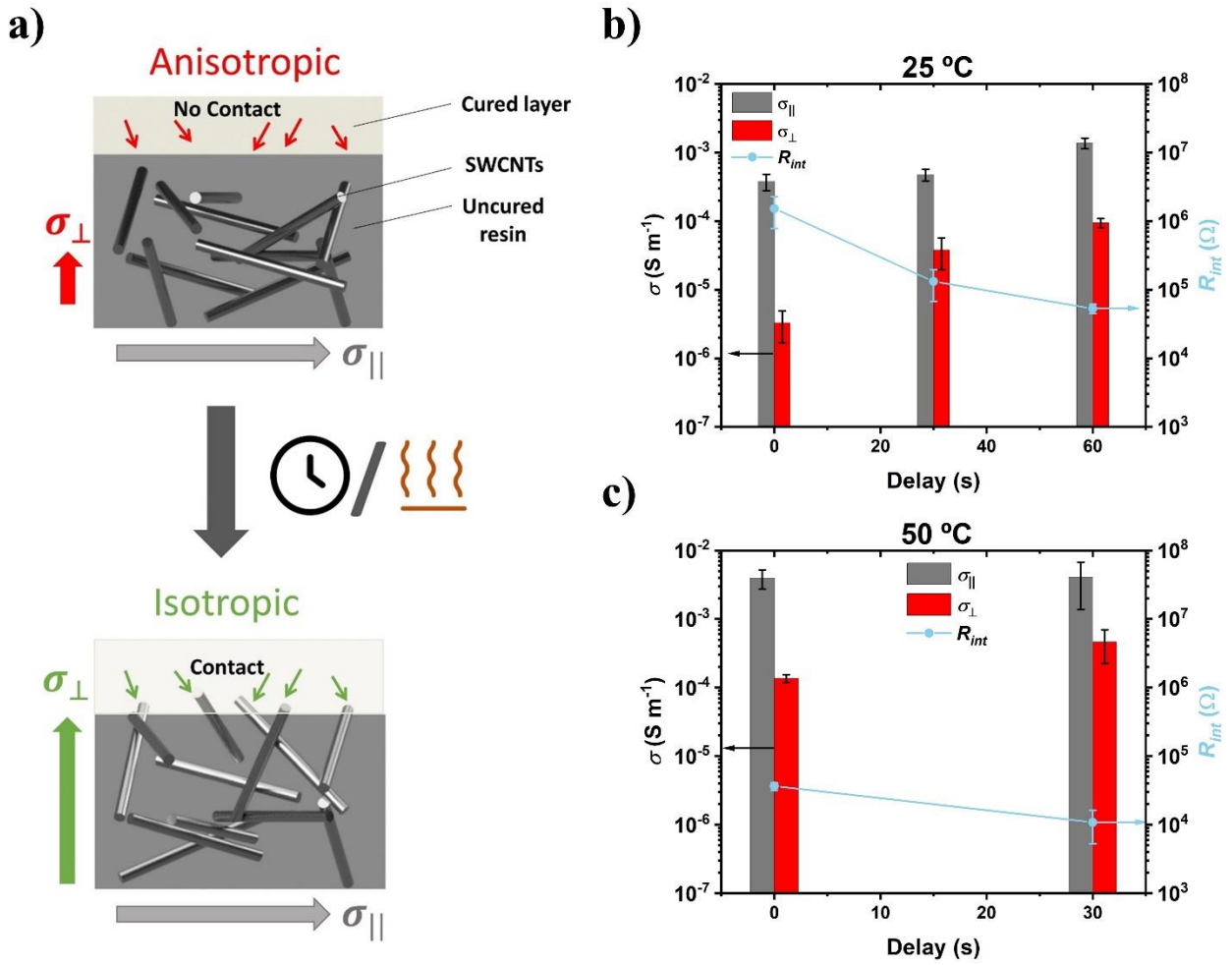

Figure 3. a) Scheme of the anisotropy mitigation by implementing a delay time once the platform is lifted down or increasing the temperature; b) Electrical conductivity parallel (grey column) and perpendicular (red column) to the layers and the interlayer resistance (blue point) versus different delay times for a 0.03 wt.% composite with a layer thickness of 20 µm (50 layers) at room temperature and c) at 50 ºC.

This issue can be addressed by decreasing the viscosity of the resin in order to accelerate the Brownian motion of the nanotubes. By increasing the temperature from 25 ºC to 50 ºC, the viscosity of the resin decreases by a factor of 4 (Supporting Information: S8), resulting in faster Brownian rotation and translation. We employed the same formulation and 3D printer and placed them in a chamber at 50 ºC to confirm the interest of operating at higher temperatures. As depicted

in Figure 3c, the composites printed at the higher temperature exhibit an increase of the parallel and perpendicular conductivities with a lower degree of anisotropy compared to those printed at room temperature. This phenomenon is attributed to the increased mobility of the tubes, which allows them to reorganize in all directions. We find $\sigma_{\perp}$= (1.4 ± 0.2) x 10^{-4} S m^{-1} and $\sigma_{\perp}$= (4.6 ± 2.3) 10^{-4} S m^{-1} for 0 and 30 seconds of delay. These values of $\sigma_{\perp}$ are greater than that of samples printed at room temperature, even with a delay of 60 s per layer (94.3 ± 14.4) x 10^{-6} S m^{-1}. Corresponding values of R_{int} are decreased down to 36.6 ± 4.8 kΩ and 10.8 ± 5.5 kΩ for 0 and 30 seconds of delay.

Conclusion

We have developed a new strategy for making 3D conductive composites by DLP and for controlling their electrical anisotropy. Surfactant-assisted SWCNT-acrylic resins have been carefully formulated in order to obtain homogeneous printable inks free of aggregates. Working curves and viscoelastic properties of the formulations have been studied to validate the 3D printability of the formulated inks. We have probed the electrical conductivity, and its anisotropy, of objects printed by DLP. The high contact resistance between printed layers explains a high electrical anisotropy of about two or three orders of magnitude for materials printed in standard conditions at room temperature. This interfacial resistance can be reduced by promoting the rotational and translational diffusion of the SWCNT from the uncured resin to the cured solid object when photo-polymerizing a layer. Diffusion is favored by implementing a delay time before UV irradiating the resin and/or increasing temperature for faster operation. These approaches allow substantial improvements of conductivity, and reduction of conductivity anisotropy below 10.

This approach shows therefore great promise for achieving high-performance, 3D printed objects with shorter manufacturing times and greater uniformity.

Methods

Materials

Tuball SWCNTs powders were purchased by OCSiAl (Luxembourg). According to the datasheet, the SWCNTs have a diameter of 1.6 ± 0.4 nm and a length 5 of µm. Disperbyk 168-TF

was purchased from BYK (Germany). According to the data sheet, the active substance is dissolved in propoxylated glyceryl triacrilate (GPTA) at 30% wt. Acrylic-based photocurable commercial resin Industrial Blend (IB) was purchased from FunToDo. Bile salts were purchased from Fluka. Isopropanol (IPA) purchased from Carlo Ebra Reagents was used as received.

Formulation

The surfactant-assisted composites were prepared as follows: Disperbyk 168-TF is added to the IB resin and dissolved by vigorous magnetic stirring for 1 hour in a light-opaque container. Then, the SWCNT powder is directly added to resin and dispersed by tip sonication. For that, a Branson digital sonifier 450 is used in order to homogenize the suspension and disrupt the CNT aggregates with a sonication tip tapped exponential horn 13 mm for 45 minutes, amplitude set to 40% with pulses of 0.5 s on, and 0.2 s off. Finally, to remove the bubbles formed during the sonication, the formulation is put under vacuum for 2 hours.

SWCNT dispersion in water for Raman polarized corrections was prepared as follows. 0.35 wt.% of bile salt surfactants was dissolved in distilled water under magnetic stirring. Then 10^{-2} wt.% of SWCNTs were added to the solution and homogenized by sonication with a tip (microtip 3.2 mm) for 30 min, an amplitude set at 15%, and pulses of 0.5 s on and 0.2 s off. The stabilization of the SWCNTs by the bile salt in water was very efficient without any aggregation or sedimentation[56].

3D printing

The IB/SWCNT formulation is poured into the tank of the DLP 3D printer Phrozen Sonic Mini 4k. This printer operates with UV irradiation at a wavelength of 405 nm.

A printing layer thickness of 20 to 100 µm is selected along with an irradiation time that depends on the SWCNT weight fraction. As explained in the supplementary information, these printing conditions have been chosen after characterizations of the working curves. The platform's lift and retract speed was 60 mm min^{-1} with a lift height of 5 mm. Once printed, the IB/SWCNT composite is soaked in an IPA bath for 15 minutes to remove the non-reticulated resin. It is then placed in a UV irradiation chamber (UltraV360) for 1 hour to complete cross-linking of the resin.

After that, the obtained IB/CNT 3D printed samples were thermally annealed in air at 200 ºC for 2h.

Characterization

The distribution of CNT inside the matrix has been qualitatively studied by TEM imaging. The thermal stability of the resin has been characterized by thermogravimetric analysis (TGA) (TA TGA 5500). About 5 mg of sample were loaded into the aluminum pan and heated from room temperature up to 200 °C, with an isothermal segment of 120 min at 200 °C. Then, it was cooled to room temperature and heated again at 300 ºC for 2h. Finally, the sample is cooled down to room temperature. All the experiments were carried out under airflow. Differential scanning calorimetry (DSC) was used to define the glass transition temperature of the resin. Experimentally, the analyses were carried out with a TA Instrument Q2000 where about 10 mg of sample was placed in a crimped aluminum crucible. Experiments are performed in an inert environment under nitrogen flow. The samples were heated from 20 °C to 240 °C at 10 °C min^{-1} and kept at 240 °C for 60 min. Then, they were cooled to room temperature at 10 °C min^{-1} and kept at 20 °C for 5 min. Three cycles were performed each time.

The formulations were poured into the printing tank, and 2x2 mm square patterns were irradiated at different times to study the working curves. The power of the LCD's 3D printer has been measured with a Thorlab PM1000A power meter. It is 1.27 mW cm^{-2}. After irradiation, the non-crosslinked formulation was rinsed and removed with 2-propanol. The thickness of the photopolymerized resin was measured with a caliper.

The rheological measurements were performed at 25ºC and 50 ºC using a controlled strain rheometer (TA AR2000) with a 40mm and 2º cone-plate geometry. The rheological tests were performed in the linear viscoelastic regime determined from steady-state flow experiments. The frequencies were in the range of 0.1 to 100 s^{-1}.

The electrical conductivity of the thermally treated composites has been measured by a two-point method using an MX24B multimeter and an impedance analyzer (7260 Impedance Analyzer, Materials Mates Italia) under a voltage of 5 V in a frequency range of 1 Hz – 10^6 Hz.

Silver paint has been used in order to ensure good electrical contact between the sample and the electrodes.

The Raman spectra were recorded using a Horiba Jobin-Yvon Xplora microscope equipped with a cooled Andor CCD detector, using excitation wavelengths of 633 nm, a laser spot size of ~ 1 μm, and an Olympus 50 x LWD objective. Raman polarized intensities denoted as I_{ij} where i is the axe polarization of the laser and j is the axe polarization of the analyzer. Besides, V stands for Vertical and H for Horizontal.

Statistical analysis:

The electrical conductivity is the mean and standard deviation of impedance spectroscopy's fits. The size of the sample is 5 for each point. For the Jacobs curves each point contains a sample size of 4 values and it is the average value ± standard deviation. For each point of the scalar nematic order parameter (S), we captured 4 Raman spectra and utilized the maximum from the Lorentz Fit as the peak for each polarization at the bottom, middle and top layer of the composite.

Funding Sources

Funding from the AID (Agence Innovation Défense) and the Nouvelle Aquitaine Region are acknowledged

Acknowledgment

We thank Prof. Eric Anglaret of the University of Montpelier for fruitful discussions and guidance for polarized Raman spectroscopy.

References

(1) Kodama, H. Automatic Method for Fabricating a Three-dimensional Plastic Model with Photo-hardening Polymer. *Review of Scientific Instruments* **1981**, *52* (11), 1770–1773. https://doi.org/10.1063/1.1136492.

(2) Lewis, J. A. Direct Ink Writing of 3D Functional Materials. *Adv. Funct. Mater.* **2006**, *16* (17), 2193–2204. https://doi.org/10.1002/adfm.200600434.

(3) Bowyer, A. 3D Printing and Humanity's First Imperfect Replicator. *3D Printing and Additive Manufacturing* **2014**, *1* (1), 4–5. https://doi.org/10.1089/3dp.2013.0003.

(4) Zohdi, N.; Yang, R. (Chunhui). Material Anisotropy in Additively Manufactured Polymers and Polymer Composites: A Review. *Polymers* **2021**, *13* (19), 3368. https://doi.org/10.3390/polym13193368.

(5) Zhang, J.; Yang, B.; Fu, F.; You, F.; Dong, X.; Dai, M. Resistivity and Its Anisotropy Characterization of 3D-Printed Acrylonitrile Butadiene Styrene Copolymer (ABS)/Carbon Black (CB) Composites. *Applied Sciences* **2017**, *7* (1), 20. https://doi.org/10.3390/app7010020.

(6) Hohimer, C. J.; Petrossian, G.; Ameli, A.; Mo, C.; Pötschke, P. 3D Printed Conductive Thermoplastic Polyurethane/Carbon Nanotube Composites for Capacitive and Piezoresistive Sensing in Soft Pneumatic Actuators. *Additive Manufacturing* **2020**, *34*, 101281. https://doi.org/10.1016/j.addma.2020.101281.

(7) Sithiprumnea Dul; Luca Fambri; Alessandro Pegoretti. Filaments Production and Fused Deposition Modelling of ABS/Carbon Nanotubes Composites. *Nanomaterials* **2018**, *8* (1), 49. https://doi.org/10.3390/nano8010049.

(8) Christ, J. F.; Aliheidari, N.; Ameli, A.; Pötschke, P. 3D Printed Highly Elastic Strain Sensors of Multiwalled Carbon Nanotube/Thermoplastic Polyurethane Nanocomposites. *Materials & Design* **2017**, *131*, 394–401. https://doi.org/10.1016/j.matdes.2017.06.011.

(9) Thaler, D.; Aliheidari, N.; Ameli, A. Mechanical, Electrical, and Piezoresistivity Behaviors of Additively Manufactured Acrylonitrile Butadiene Styrene/Carbon Nanotube Nanocomposites. *Smart Mater. Struct.* **2019**, *28* (8), 084004. https://doi.org/10.1088/1361-665X/ab256e.

(10) Gnanasekaran, K.; Heijmans, T.; van Bennekom, S.; Woldhuis, H.; Wijnia, S.; de With, G.; Friedrich, H. 3D Printing of CNT- and Graphene-Based Conductive Polymer Nanocomposites by Fused Deposition Modeling. *Applied Materials Today* **2017**, *9*, 21–28. https://doi.org/10.1016/j.apmt.2017.04.003.

(11) Tilve-Martinez, D.; Neri, W.; Horaud, D.; Vukadinovic, N.; Berton, B.; Desmedt, A.; Yuan, J.; Poulin, P. G Raphene O Xide B Ased T Ransparent R Esins F or A Ccurate 3D P Rinting of C Onductive M Aterials. *Adv Funct Materials* **2023**, 2214954. https://doi.org/10.1002/adfm.202214954.

(12) Gundrati, N. B.; Chakraborty, P.; Zhou, C.; Chung, D. D. L. First Observation of the Effect of the Layer Printing Sequence on the Molecular Structure of Three-Dimensionally Printed Polymer, as Shown by in-Plane Capacitance Measurement. *Composites Part B: Engineering* **2018**, *140*, 78–82. https://doi.org/10.1016/j.compositesb.2017.12.008.

(13) Chakraborty, P.; Zhao, G.; Zhou, C.; Chung, D. D. L. Unprecedented Sensing of Interlayer Defects in Three-Dimensionally Printed Polymer by Capacitance Measurement. *Smart Mater. Struct.* **2018**, *27* (11), 115012. https://doi.org/10.1088/1361-665X/aae16e.

(14) Vigolo, B.; Coulon, C.; Maugey, M.; Zakri, C.; Poulin, P. An Experimental Approach to the Percolation of Sticky Nanotubes. *Science* **2005**, *309* (5736), 920–923. https://doi.org/10.1126/science.1112835.
(15) Schilling, T.; Jungblut, S.; Miller, M. A. Depletion-Induced Percolation in Networks of Nanorods. *Phys. Rev. Lett.* **2007**, *98* (10), 108303. https://doi.org/10.1103/PhysRevLett.98.108303.
(16) Meyer, H.; van der Schoot, P.; Schilling, T. Percolation in Suspensions of Polydisperse Hard Rods: Quasi Universality and Finite-Size Effects. *The Journal of Chemical Physics* **2015**, *143* (4), 044901. https://doi.org/10.1063/1.4926946.
(17) Kyrylyuk, A. V.; van der Schoot, P. Continuum Percolation of Carbon Nanotubes in Polymeric and Colloidal Media. *Proceedings of the National Academy of Sciences* **2008**, *105* (24), 8221–8226. https://doi.org/10.1073/pnas.0711449105.
(18) Balberg, I.; Binenbaum, N.; Wagner, N. Percolation Thresholds in the Three-Dimensional Sticks System. *Phys. Rev. Lett.* **1984**, *52* (17), 1465–1468. https://doi.org/10.1103/PhysRevLett.52.1465.
(19) Celzard, A.; McRae, E.; Deleuze, C.; Dufort, M.; Furdin, G.; Marêché, J. F. Critical Concentration in Percolating Systems Containing a High-Aspect-Ratio Filler. *Phys. Rev. B* **1996**, *53* (10), 6209–6214. https://doi.org/10.1103/PhysRevB.53.6209.
(20) De Volder, M. F. L.; Tawfick, S. H.; Baughman, R. H.; Hart, A. J. Carbon Nanotubes: Present and Future Commercial Applications. *Science* **2013**, *339*, 535–539.
(21) Dresselhaus, G.; Dresselhaus, M. S.; Saito, R. *Physical Properties of Carbon Nanotubes*; IMPERIAL COLLEGE PRESS, 1998.
(22) Ebbesen, T. W.; Lezec, H. J.; Hiura, H.; Bennett, J. W.; Ghaemi, H. F.; Thio, T. Electrical Conductivity of Individual Carbon Nanotubes. *Nature* **1996**, *382* (6586), 54–56.
(23) Snow, E. S.; Novak, J. P.; Campbell, P. M.; Park, D. Random Networks of Carbon Nanotubes as an Electronic Material. *Applied Physics Letters* **2003**, *82* (13), 2145–2147.
(24) Kobashi, K.; Ata, S.; Yamada, T.; Futaba, D. N.; Okazaki, T.; Hata, K. Classification of Commercialized Carbon Nanotubes into Three General Categories as a Guide for Applications. *ACS Appl. Nano Mater.* **2019**, *2* (7), 4043–4047. https://doi.org/10.1021/acsanm.9b00941.
(25) Cortés, A.; Cosola, A.; Sangermano, M.; Campo, M.; González Prolongo, S.; Pirri, C. F.; Jiménez-Suárez, A.; Chiappone, A. DLP 4D-Printing of Remotely, Modularly, and Selectively Controllable Shape Memory Polymer Nanocomposites Embedding Carbon Nanotubes. *Adv. Funct. Mater.* **2021**, *31* (50), 2106774. https://doi.org/10.1002/adfm.202106774.
(26) Gonzalez, G.; Chiappone, A.; Roppolo, I.; Fantino, E.; Bertana, V.; Perrucci, F.; Scaltrito, L.; Pirri, F.; Sangermano, M. Development of 3D Printable Formulations Containing CNT with Enhanced Electrical Properties. *Polymer* **2017**, *109*, 246–253. https://doi.org/10.1016/j.polymer.2016.12.051.
(27) Saadi, O. W.; Schiffer, A.; Kumar, S. Piezoresistive Behavior of DLP 3D Printed CNT/Polymer Nanocomposites under Monotonic and Cyclic Loading. *Int J Adv Manuf Technol* **2023**. https://doi.org/10.1007/s00170-023-11123-8.
(28) Mu, Q.; Wang, L.; Dunn, C. K.; Kuang, X.; Duan, F.; Zhang, Z.; Qi, H. J.; Wang, T. Digital Light Processing 3D Printing of Conductive Complex Structures. *Additive Manufacturing* **2017**, *18*, 74–83. https://doi.org/10.1016/j.addma.2017.08.011.

(29) Maillaud, L.; Zakri, C.; Ly, I.; Pénicaud, A.; Poulin, P. Conductivity of Transparent Electrodes Made from Interacting Nanotubes. *Appl. Phys. Lett.* **2013**, *103* (26), 263106. https://doi.org/10.1063/1.4858215.
(30) Arjmand, M.; Mahmoodi, M.; Gelves, G. A.; Park, S.; Sundararaj, U. Electrical and Electromagnetic Interference Shielding Properties of Flow-Induced Oriented Carbon Nanotubes in Polycarbonate. *Carbon* **2011**, *49* (11), 3430–3440. https://doi.org/10.1016/j.carbon.2011.04.039.
(31) *Fundamental and Applied Nano-Electromagnetics*; Maffucci, A., Maksimenko, S. A., Eds.; NATO Science for Peace and Security Series B: Physics and Biophysics; Springer Netherlands: Dordrecht, 2016. https://doi.org/10.1007/978-94-017-7478-9.
(32) Sun, H.; Che, R.; You, X.; Jiang, Y.; Yang, Z.; Deng, J.; Qiu, L.; Peng, H. Cross-Stacking Aligned Carbon-Nanotube Films to Tune Microwave Absorption Frequencies and Increase Absorption Intensities. *Adv. Mater.* **2014**, *26* (48), 8120–8125. https://doi.org/10.1002/adma.201403735.
(33) Nanni, F.; Mayoral, B. L.; Madau, F.; Montesperelli, G.; McNally, T. Effect of MWCNT Alignment on Mechanical and Self-Monitoring Properties of Extruded PET–MWCNT Nanocomposites. *Composites Science and Technology* **2012**, *72* (10), 1140–1146. https://doi.org/10.1016/j.compscitech.2012.03.015.
(34) Böger, L.; Wichmann, M. H. G.; Meyer, L. O.; Schulte, K. Load and Health Monitoring in Glass Fibre Reinforced Composites with an Electrically Conductive Nanocomposite Epoxy Matrix. *Composites Science and Technology* **2008**, *68* (7–8), 1886–1894. https://doi.org/10.1016/j.compscitech.2008.01.001.
(35) Blackburn, J. L.; Ferguson, A. J.; Cho, C.; Grunlan, J. C. Carbon-Nanotube-Based Thermoelectric Materials and Devices. *Adv. Mater.* **2018**, *30* (11), 1704386. https://doi.org/10.1002/adma.201704386.
(36) Wang, Z.-G.; Yang, Y.-L.; Zheng, Z.-L.; Lan, R.-T.; Dai, K.; Xu, L.; Huang, H.-D.; Tang, J.-H.; Xu, J.-Z.; Li, Z.-M. Achieving Excellent Thermally Conductive and Electromagnetic Shielding Performance by Nondestructive Functionalization and Oriented Arrangement of Carbon Nanotubes in Composite Films. *Composites Science and Technology* **2020**, *194*, 108190. https://doi.org/10.1016/j.compscitech.2020.108190.
(37) Miaudet, P.; Badaire, S.; Maugey, M.; Derré, A.; Pichot, V.; Launois, P.; Poulin, P.; Zakri, C. Hot-Drawing of Single and Multiwall Carbon Nanotube Fibers for High Toughness and Alignment. *Nano Lett.* **2005**, *5* (11), 2212–2215. https://doi.org/10.1021/nl051419w.
(38) Miaudet, P.; Bartholome, C.; Derre, A.; Maugey, M.; Sigaud, G.; Zakri, C.; Poulin, P. Thermo-Electrical Properties of PVAenanotube Composite Fibers. *Polymer* **2007**, *48*, 4068–4074.
(39) Bartholome, C.; Miaudet, P.; Derre, A.; Maugey, M.; Roubeau, O.; Zakri, C.; Poulin, P. Influence of Surface Functionalization on the Thermal and Electrical Properties of Nanotube–PVA Composites. *Compos. Sci. Technol.* **2008**, *68*, 2568–2573.
(40) Kymakis, E.; Amaratunga, G. A. J. Electrical Properties of Single-Wall Carbon Nanotube-Polymer Composite Films. *Journal of Applied Physics* **2006**, *99* (8), 084302. https://doi.org/10.1063/1.2189931.
(41) Kilbride, B. E.; Coleman, J. N.; Fraysse, J.; Fournet, P.; Cadek, M.; Drury, A.; Hutzler, S.; Roth, S.; Blau, W. J. Experimental Observation of Scaling Laws for Alternating Current and Direct Current Conductivity in Polymer-Carbon Nanotube Composite Thin Films. *Journal of Applied Physics* **2002**, *92* (7), 4024–4030. https://doi.org/10.1063/1.1506397.

(42) Abbasi, H.; Antunes, M.; Velasco, J. I. Recent Advances in Carbon-Based Polymer Nanocomposites for Electromagnetic Interference Shielding. *Progress in Materials Science* **2019**, *103*, 319–373. https://doi.org/10.1016/j.pmatsci.2019.02.003.
(43) Balberg, I.; Anderson, C. H.; Alexander, S.; Wagner, N. Excluded Volume and Its Relation to the Onset of Percolation. *Phys. Rev. B* **1984**, *30* (7), 3933–3943. https://doi.org/10.1103/PhysRevB.30.3933.
(44) Stauffer, D.; Aharony, A. *Introduction to Percolation Theory*; CRC press, 2018.
(45) Roman, J.; Neri, W.; Fierro, V.; Celzard, A.; Bentaleb, A.; Ly, I.; Zhong, J.; Derré, A.; Poulin, P. Lignin-Graphene Oxide Inks for 3D Printing of Graphitic Materials with Tunable Density. *Nano Today* **2020**, *33*, 100881. https://doi.org/10.1016/j.nantod.2020.100881.
(46) Chen, J.; Liu, X.; Tian, Y.; Zhu, W.; Yan, C.; Shi, Y.; Kong, L. B.; Qi, H. J.; Zhou, K. 3D-Printed Anisotropic Polymer Materials for Functional Applications. *Advanced Materials* **2022**, *34* (5), 2102877. https://doi.org/10.1002/adma.202102877.
(47) Puech, N.; Blanc, C.; Grelet, E.; Zamora-Ledezma, C.; Maugey, M.; Zakri, C.; Anglaret, E.; Poulin, P. Highly Ordered Carbon Nanotube Nematic Liquid Crystals. *J. Phys. Chem. C* **2011**, *115* (8), 3272–3278. https://doi.org/10.1021/jp1102077.
(48) Zamora-Ledezma, C.; Blanc, C.; Maugey, M.; Zakri, C.; Poulin, P.; Anglaret, E. Anisotropic Thin Films of Single-Wall Carbon Nanotubes from Aligned Lyotropic Nematic Suspensions. *Nano Lett.* **2008**, *8* (12), 4103–4107. https://doi.org/10.1021/nl801525x.
(49) Torres-Canas, F.; Blanc, C.; Mašlík, J.; Tahir, S.; Izard, N.; Karasahin, S.; Castellani, M.; Dammasch, M.; Zamora-Ledezma, C.; Anglaret, E. Morphology and Anisotropy of Thin Conductive Inkjet Printed Lines of Single-Walled Carbon Nanotubes. *Mater. Res. Express* **2017**, *4* (3), 035037. https://doi.org/10.1088/2053-1591/aa5687.
(50) Anglaret, E.; Righi, A.; Sauvajol, J. L.; Bernier, P.; Vigolo, B.; Poulin, P. Raman Study of Orientational Order in Fibers of Single Wall Carbon Nanotubes. *Physica B: Condensed Matter* **2002**, *323* (1–4), 38–43. https://doi.org/10.1016/S0921-4526(02)00962-6.
(51) Hu, L.; Hecht, D. S.; Grüner, G. Percolation in Transparent and Conducting Carbon Nanotube Networks. *Nano Lett.* **2004**, *4* (12), 2513–2517. https://doi.org/10.1021/nl048435y.
(52) Keblinski, P.; Cleri, F. Contact Resistance in Percolating Networks. *Phys. Rev. B* **2004**, *69* (18), 184201. https://doi.org/10.1103/PhysRevB.69.184201.
(53) Žeželj, M.; Stanković, I. From Percolating to Dense Random Stick Networks: Conductivity Model Investigation. *Phys. Rev. B* **2012**, *86* (13), 134202. https://doi.org/10.1103/PhysRevB.86.134202.
(54) Sandler, J. K. W.; Kirk, J. E.; Kinloch, I. A.; Shaffer, M. S. P.; Windle, A. H. Ultra-Low Electrical Percolation Threshold in Carbon-Nanotube-Epoxy Composites. *Polymer* **2003**, *44* (19), 5893–5899. https://doi.org/10.1016/S0032-3861(03)00539-1.
(55) Doi, M. Rotational Relaxation Time of Rigid Rod-like Macromolecule in Concentrated Solution. *J. Phys. France* **1975**, *36* (7–8), 607–611. https://doi.org/10.1051/jphys:01975003607-8060700.
(56) Wenseleers, W.; Vlasov, I. I.; Goovaerts, E.; Obraztsova, E. D.; Lobach, A. S.; Bouwen, A. Efficient Isolation and Solubilization of Pristine Single-Walled Nanotubes in Bile Salt Micelles. *Adv. Funct. Mater.* **2004**, *14* (11), 1105–1112. https://doi.org/10.1002/adfm.200400130.